# Crossover effects in chemical-dissolution phenomena: A renormalization-group study

Takashi Nagatani
*Center for Polymer Studies and Department of Physics, Boston University, Boston, Massachusetts 02215 and College of Engineering, Shizuoka University, Hamamatsu 432, Japan*

Jysoo Lee* and H. Eugene Stanley
*Center for Polymer Studies and Department of Physics, Boston University, Boston, Massachusetts 02215*
(Received 12 July 1991; revised manuscript received 13 September 1991)

We study the patterns formed when a reactive fluid with viscosity $\mu$ is injected into a two-dimensional porous medium filled with a nonreactive fluid with unit viscosity. We consider the "mass-transfer limit," where the time scale of chemical reaction between the injected fluid and porous medium is much smaller than the time scale of reactant transport. Also, the surface tension between two fluids is ignored. We formulate three-parameter position-space-renormalization-group equations for this system. We find two crossovers: (i) from the first diffusion-limited-aggregation (DLA) fixed point to the Eden fixed point due to finite viscosity, and (ii) from the Eden to the second DLA due to chemical dissolution. The time evolution between patterns is independent of the injection rate following a trivial rescaling of time. These results are checked by direct numerical simulations. The second crossover is characterized by the crossover radius $r_c \sim v^{-1/\beta\phi}$, where $v$ is the total volume of the injected fluid, and $\beta=\frac{3}{2}$, $\phi \cong 1.63$. We also study the effect of consumption of the reactant, and find that it stabilizes the pattern from a DLA fractal to a compact shape.

PACS number(s): 68.70.+w, 05.40.+j, 47.70.Fw

## I. INTRODUCTION

The formation of dissolution patterns by injecting a reactive fluid into a soluble porous medium filled with a nonreactive fluid has been investigated by both experimental and computational methods [1,2]. Daccord and Lenormand [1,2] have found that when high injection rates are used, the pattern formed by the chemical-dissolution process yields a diffusion-limited-aggregation (DLA) fractal [3]. The underlying mechanism for the formation of dissolution patterns couples (i) the flow of the liquid into the porous medium with (ii) the chemical reaction between the injected fluid and the medium. Daccord [1] has proposed a simulation model that introduces a cumulative erosion process, which broadens the branches of the cluster. The patterns obtained from the simulations are very similar to the experimental ones. Questions that remain open include (i) the asymptotic behavior of the dissolution patterns and (ii) the relevance of such parameters as injection rate, viscosity of the injected fluid, and concentration of the reactant.

Very recently, the crossover from a DLA fractal to a dense structure for viscous fingering with nonzero viscosity ratio has been studied using a two-parameter position-space-renormalization-group (PSRG) method [4]. Also, Nagatani [5] analyzed the effect of the sticking probability on the fractal structure of DLA. When the sticking probability is not zero, the aggregate crosses over to DLA as the mass approaches infinity. The combined effect of the sticking probability and the finite viscosity ratio was analyzed using a three-parameter PSRG method [6]. A double-crossover phenomena was found—from the dense pattern, through the DLA fractal, and finally to the dense structure. Furthermore, the morphological changes of viscous fingering in porous media were analyzed using the renormalization-group method [7]. Two double-crossover phenomena were found: (i) when $\mu \ll (p-p_c) \ll 1$, the double crossover occurs from DLA on an incipient percolation cluster through DLA on the perfect lattice to the dense structure, and (ii) when $1 \gg \mu \gg (p-p_c)$ the other double crossover appears from DLA on an incipient percolation cluster through invasion percolation to a dense structure, where $p_c$ is the percolation threshold.

In a recent Letter [8], we reported preliminary results on chemical dissolution in the mass-transfer limit by developing a three-parameter PSRG method. We considered the combined effect of finite viscosity ratio $\mu$ and chemical dissolution on the pattern. We found that the asymptotic behavior in this problem is characterized by two distinct crossovers: (i) one from DLA clusters to compact clusters (due to the finite viscosity ratio), and (ii) a second crossover from compact clusters to DLA clusters (due to the chemical dissolution). It was also found that the second crossover is characterized by the crossover radius $r_c \sim v^{-1/\beta\phi}$, with $\beta=\frac{3}{2}$ and $\phi \cong 1.63$. Here we present the details of the calculation. Specifically, we show how to form the PSRG equations, and how to analyze the equations to obtain desired information (crossovers between the patterns and the crossover exponent). Furthermore, we also present additional studies on the effect of consumption of the reactant. We find that consumption tends to stabilize the pattern and cause the crossover from a DLA fractal to a compact pattern.

The organization of this paper is as follows. In Sec. II we present the basic equations used in our models. In

Sec. III we analyze the crossover phenomena in viscous fingering with chemical dissolution using a three-parameter PSRG method. In Sec. IV we examine how the consumption of the reactant affects the pattern. In Sec. V we show the results of the computer simulation. In Sec. VI we present a brief summary.

## II. MODEL AND BASIC EQUATIONS

We consider the formation of dissolution patterns by injecting a reactive fluid of viscosity $\mu$ into a soluble porous medium filled with a nonreactive fluid of unit viscosity. Pattern formation by reactive injection fluid must be studied in two separate regimes [9]. One regime is when the time scale of the chemical reaction is much shorter than the time scales of the fluid motion (convection and diffusion). We call this regime the "mass-transfer-limited" regime, since the speed of the chemical reaction is controlled by the supply of the reactive fluid. The other regime, where the time scale of the chemical reaction is much larger, is called the "reaction-limited" regime.

In this paper we study only the mass-transfer-limited regime. We also ignore the surface tension effects between the two fluids. The chemical dissolution is described by the equations

$$M_D \nabla^2 P_D = 0 , \tag{1a}$$

for the displaced fluid, and

$$\nabla \cdot [M_I(x,t) \nabla P_I] = 0 , \tag{1b}$$

for the injected fluid. Here $P_D$ and $P_I$ are the pressures of the displaced fluid and the injected fluid, $M_D$ the mobility of the displaced fluid, and $M_I(x,t)$ the mobility of the injected fluid, which is dependent upon position and time. The mobility of the injected fluid is governed by the cumulative erosion process.

We propose that the time evolution of the mobility is given by an equation similar to that used in Ref. [1],

$$M_I(x,t) = \mu^{-1}(1+\{q[t-t_0(x)]\}^{\beta}) . \tag{2}$$

Here $t$ is the time, $t_0(x)$ the time when the injected fluid touches a site at position $x$, $\mu$ the viscosity of the injected fluid, and $q$ the flow rate. In Ref. [1] it is argued that the parameter $\beta$ is $\frac{3}{2}$ if the dissolution kinetics is limited by molecular diffusion. Equation (2) can be used to describe a cumulative erosion process that broadens the branches of the cluster. In general, $q$ can be generalized to be dependent on the concentration of the reactant and the reaction rate. However, Eq. (2) is not the *only* choice for the time development of $M_I$. Consider that the reactant is transferred by diffusion in laminar flow in a tube.

If we assume that a pore within a porous medium is a tube with a radius $R$, the flux of the dissolving substance is given by

$$j = D \left[ \frac{\partial c}{\partial r} \right]_{r=R} \simeq 0.67 c_0 D \left[ \frac{v_m}{DRl} \right]^{1/3} ,$$

where $D$ is the diffusion constant, $c$ is the concentration field of the reactant, $c_0$ the average concentration of reactant, $v_m$ the mean velocity, and $l$ the distance from the inlet [10]. We assumed here that the concentration at the surface of the pore is always equal to zero because the surface chemical reaction is much faster than the time scale of the mass transfer. The time evolution of the pore size is given by

$$\frac{dR}{dt} = \frac{j}{\rho_s} ,$$

where $\rho_s$ is the density of the porous medium. The mobility of the injected fluid is proportional to the square of the pore size. The mobility of the injected fluid is given by

$$M = a \left[ 1 + \frac{\Delta R}{R_0} \right]^2 , \tag{3}$$

where $a$ is the initial mobility of the injected fluid, $R_0$ the initial radius of the pore, and $\Delta R$ the increment of the pore radius. The initial mobility $a$ is proportional to the inverse $\mu^{-1}$ of the viscosity. Using the above relations, the mobility is described by

$$M = a(1+\{q[t-t_0(x)]\}^{\beta/2})^2 , \tag{4}$$

with

$$q \simeq 0.89 \left[ \frac{c_0}{\rho_s} \right] \left[ \frac{v_m D^2}{R_0^4 l} \right]^{1/3} .$$

Here $t$ is time, and $t_0(x)$ dimensionless time when a tip of the finger touches site $x$. The pore size of the cluster increases with time after the injection fluid reaches point $x$.

The form of the mobility presented in Eq. (4) can also be used to describe a cumulative erosion process. The mobility of the injected fluid increases with time $t$. Although we assume that the concentration $c_0$ of the reactive fluid is constant, in the later stages of the dissolution process, the dissolving power is actually limited by the finite concentration of the reactant. The pore size of the branches is not able to increase for very long due to consumption of the reactant. This effect of the finite concentration is discussed in Sec. IV. Logically, we would expect that a finite concentration would stabilize the pattern, i.e., favor the Eden limit. The boundary conditions on the interface are given by

$$\begin{aligned} P_D &= P_I , \\ v_n &= -M_D \mathbf{n} \cdot \nabla P_D \\ &= -M_I \mathbf{n} \cdot \nabla P_I , \end{aligned} \tag{5}$$

where $v_n$ is the normal velocity of the interface and $\mathbf{n}$ the unit vector normal to the interface. Without loss of generality, we set $M_D = 1$. The models given in Eqs. (2) and (4) [model A and model B, respectively] can be applied to the mass-transfer-limited regime. In the reaction-limited regime, the time scale of the chemical reaction is much larger than those of the fluid motions (convection and diffusion). Therefore, after the viscous finger grows sufficiently, the chemical dissolution process occurs in the

area occupied by the reactive injection fluid. The pores occupied by the reactive injection fluid become larger.

## III. RENORMALIZATION-GROUP APPROACH

In both models A and B, we study pattern formation in viscous fingering caused by chemical dissolution by means of the position-space-renormalization-group method. Using the resistor-network model to describe the viscous-fingering problem (pressure, flow rate, and mobility in viscous fingering corresponding to voltage, current, and conductance in a resistor network), we induce morphological change by varying the viscosity of the injected fluid and the rate of injection. For simplicity, we consider the renormalization procedure on a diamond hierarchical lattice: each bond is occupied by a resistor of unit conductance, and a constant current $q$ is applied across the diamond hierarchical lattice. We distinguish the following three types of bonds (Fig. 1): (1) injected fluid bonds (thick lines that form clusters); (2) growth bonds (wavy lines on the perimeter of the cluster); and (3) displaced fluid bonds (thin lines).

The conductances of the injected, growth, and displaced bonds are $\sigma_I$, $\sigma_G$, and 1, respectively. We now shall derive the renormalization-group equations for the conductances of the surface and injected bonds, for the total current, and for the time increment.

We partition the whole cluster into cells of size 2, and replace these cells with "renormalized" bonds. The $n$th generation of the diamond lattice is transformed into an $(n-1)$th generation. When the injected bonds span the cell, we renormalize into an injected bond. When the injected bonds do not span the cell, we renormalize into a growth bond. If a cell does not contain an injected and growth bond, we renormalize into a displaced bond. The renormalization transformation of the surface bonds constitutes the first of the renormalization equations,

$$\sigma'_G=\mathcal{R}_G(\sigma_G,\sigma_I,\Delta t,q) . \tag{6}$$

$\mathcal{R}_G$ is calculated as the average conductance of all the nonspanning configurations that contain injected bonds. The time increment $\Delta t$ is defined as the time period for the displacement of one injected bond. The second renormalization equation is the renormalization transformation for the conductance of injected bonds,

$$\sigma'_I=\mathcal{R}_I(\sigma_G,\sigma_I,\Delta t,q) . \tag{7}$$

$\mathcal{R}_I$ is calculated as the average conductance of all the spanning configurations that contain injected bonds. Furthermore, the time increment $\Delta t$ is renormalized to be a time period $\Delta t'$ during which the breakdown within the cell proceeds from the bottom to the top. The third equation is the renormalization transformation of the time increment,

$$\Delta t'=\mathcal{R}_t(\sigma_G,\sigma_I,\Delta t,q) . \tag{8}$$

Also, the renormalization equation for the total current is $q'=2q$.

Equations (6)–(8) give the renormalization-group equations, which have been derived explicitly. Figure 1 shows the growth process within a cell, which we assume to be stepwise: the growth proceeds one step at a time, and at any given time only one bond is growing (there is no simultaneous bond growth). The configuration in Fig. 1(a) shows a cell in which the growth has just reached the bottom. Configuration 1(b) is constructed by replacing a growth bond in configuration 1(a) with an injected bond 1 or 2. The probability of an injected bond adding to the growth bonds 1 or 2 in configuration 1(a) is given by the growth probabilities $p_{a,1}$ or $p_{a,2}$ of the growth bonds 1 or 2 in configuration 1(a). In like fashion, if an injected bond is added to configuration 1(b), configurations 1(c) and (1) result. The time increases by time increment $\Delta t$. The conductance of the fully grown bond (injected bond) then increases [see Eqs. (2) and (4)],

$$\sigma_I\rightarrow\sigma_I[1+(q\Delta t)^{\beta}] , \tag{9a}$$

$$\sigma_I\rightarrow\sigma_I[1+(q\Delta t)^{\beta/2}]^2 . \tag{9b}$$

We actually show two expressions for models A and B [(9a) and (9b)] only when the results are different. As the growth continues, either configuration (2) or configuration (3) occurs. As the time increases, the conductances of the fully grown bond (injected bond) increase as

$$\sigma_I\rightarrow\sigma_I[1+(q\Delta t)^{\beta}]\rightarrow\sigma_I[1+(2q\Delta t)^{\beta}] , \tag{10a}$$

$$\sigma_I\rightarrow\sigma_I[1+(q\Delta t)^{\beta/2}]^2\rightarrow\sigma_I[1+(2q\Delta t)^{\beta/2}]^2 . \tag{10b}$$

In Fig. 1 each injected bond is labeled by a number (1,2,3,4) that designates its order in the growth process,

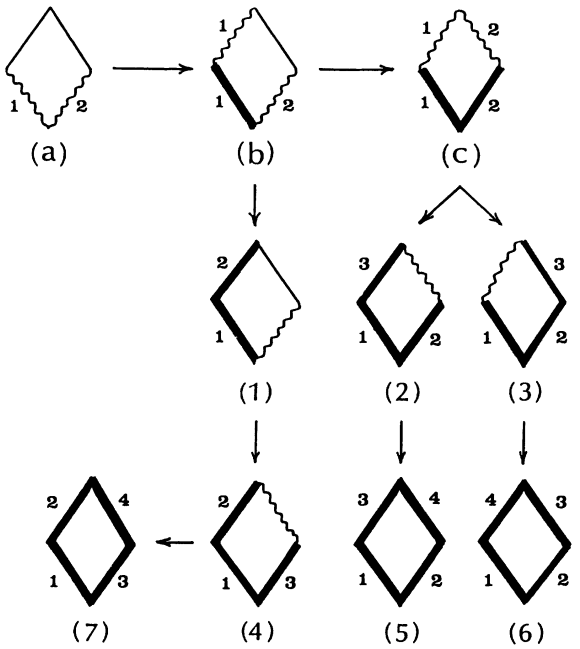


FIG. 1. All distinct configurations of the cell. The configurations (a), (b), and (c) are renormalized to the growth bonds. The configurations (1)–(7) are renormalized to the injected bonds. The thick, wavy, and thin lines indicate, respectively, the injected, growth, and displaced bonds.

and each grows according to these numbers. As the step-by-step growth process continues, the conductance of the injected bond—described by either Eq. (2) or Eq. (4)—increases with time.

Cell configurations (a)–(c) in Fig. 1 are all the configurations that can be renormalized as growth bonds. Configurations (1)–(7) are all that can be renormalized as injected bonds. Configurations (1)–(7) of Fig. 1 give all possible configurations of the spanning cluster.

Let us consider $C_\alpha$ ($\alpha=a,b,c,1-7$), the probability that a particular configuration $\alpha$ will appear. Here, the configurational probabilities are normalized, respectively, as 1 for renormalized growth bonds and for renormalized injected bonds. The configurational probabilities $C_\alpha$ ($\alpha=a,b,c$) are given by (see Refs. [4]–[6] for details)

$$C_a=1-C_b-C_c \ , \tag{11a}$$

$$C_b=C_a(p_{a,1}+p_{a,2}) \ , \tag{11b}$$

$$C_c=C_b p_{b,2} \ , \tag{11c}$$

where $p_{a,i}$ is the transition probability of the growth bond $i$ to become an injected bond $i$ within a cell (a). Growth probability $p_{a,i}$ is proportional to the current passing through growth bond $i$, and is given by

$$p_{a,1}=p_{a,2}=\tfrac{1}{2} \ , \tag{12}$$

$$p_{b,1}=\tfrac{1}{2} \ , \tag{13}$$

$$p_{b,2}=1-p_{b,1} \ , \tag{14}$$

$$p_{c,1}=\tfrac{1}{2} \ , \tag{15}$$

$$p_{c,2}=1-p_{c,1} \ . \tag{16}$$

The surface conductance $\sigma'_{G,\alpha}$ of a cell with configuration $\alpha$ is renormalized as follows:

$$\sigma'_{G,a}=2(1+\sigma_G^{-1})^{-1} \ , \tag{17}$$

$$\sigma'_{G,b}=(1+\sigma_G^{-1})^{-1}+(\sigma_I^{-1}+\sigma_G^{-1})^{-1} \ , \tag{18}$$

$$\sigma'_{G,c}=(\sigma_I^{-1}+\sigma_G^{-1})^{-1} +\{\sigma_I^{-1}[1+(q\Delta t)^{\beta}]^{-1}+\sigma_G^{-1}\}^{-1} \ , \tag{19a}$$

$$\sigma'_{G,c}=(\sigma_I^{-1}+\sigma_G^{-1})^{-1} +\{\sigma_I^{-1}[1+(q\Delta t)^{\beta/2}]^{-2}+\sigma_G^{-1}\}^{-1} \ . \tag{19b}$$

The renormalized conductance $\sigma'_G$ of the growth bond can be given as either an algebraic or a geometric average; the difference between the two averages not having a qualitative effect on crossover phenomena [4]. Here, we choose the algebraic average [11] for the renormalized conductance of the growth bond,

$$\sigma'_G=C_a\sigma'_{G,a}+C_b\sigma'_{G,b}+C_c\sigma'_{G,c} \ . \tag{20}$$

Relationships (17)–(20) present the renormalization equation (6). In the limit of infinite-viscosity ratio ($\sigma_I\to\infty$), Eqs. (17)–(20) reduce to those of an injected fluid with zero viscosity.

We now consider the renormalization of conductance $\sigma_I$ for the spanning cluster to be renormalized as the injected bond. Configurations (1)–(7) in Fig. 1 show all the spanning clusters. Configurations (1)–(7) of the spanning cluster are constructed from the configurations of the growth cell on the top side. Configuration (1) in Fig. 1 is constructed by adding an injected bond onto a growth bond 1 in configuration 1(b). The configurational probability $C_1$ of configuration (1) is given by

$$C_1=C_0 p_{b,1}C_b \ . \tag{21}$$

Configurations (2) and (3) of Fig. 1 are constructed by adding an injected bond to growth bonds 1 or 2 in configuration 1(c). The configurational probabilities $C_2$ and $C_3$ are given by

$$\begin{aligned} C_2&=C_0 p_{c,1}C_c \ , \\ C_3&=C_0 p_{c,2}C_c \ . \end{aligned} \tag{22}$$

Furthermore, the cluster grows and configurations (4)–(7) in Fig. 1 occur. The configurational probabilities $C_4$–$C_7$ are given by

$$C_4=C_1 \ , \tag{23a}$$

$$C_5=C_2 \ , \tag{23b}$$

$$C_6=C_3 \ , \tag{23c}$$

$$C_7=C_4 \ . \tag{23d}$$

The unknown constant $C_0$ is determined by the normalization condition

$$\sum_{i=1}^{7} C_i=1 \ . \tag{23e}$$

Conductances $\sigma'_{I,1}$-$\sigma'_{I,7}$ of the cell in configurations (1)–(7) in Fig. 1 are given by

$$\sigma'_{I,1}=\frac{1}{1+\sigma_G^{-1}}+\frac{\sigma_I}{1+[1+(q\Delta t)^{\beta}]^{-1}} \ , \tag{24a}$$

$$\sigma'_{I,1}=\frac{1}{1+\sigma_G^{-1}}+\frac{\sigma_I}{1+[1+(q\Delta t)^{\beta/2}]^{-2}} \ , \tag{24b}$$

$$\sigma'_{I,2}=\frac{\sigma_I}{\sigma_I\sigma_G^{-1}+[1+(q\Delta t)^{\beta}]^{-1}} +\frac{\sigma_I}{1+[1+(2q\Delta t)^{\beta}]^{-1}} \ , \tag{25a}$$

$$\sigma'_{I,2}=\frac{\sigma_I}{\sigma_I\sigma_G^{-1}+[1+(q\Delta t)^{\beta/2}]^{-2}} +\frac{\sigma_I}{1+[1+(2q\Delta t)^{\beta/2}]^{-2}} \ , \tag{25b}$$

$$\sigma'_{I,3}=\frac{\sigma_I}{\sigma_I\sigma_G^{-1}+[1+(2q\Delta t)^{\beta}]^{-1}} +\frac{\sigma_I}{1+[1+(q\Delta t)^{\beta}]^{-1}} \ , \tag{26a}$$

$$\sigma'_{I,3}=\frac{\sigma_I}{\sigma_I\sigma_G^{-1}+[1+(2q\Delta t)^{\beta/2}]^{-2}}+\frac{\sigma_I}{1+[1+(q\Delta t)^{\beta/2}]^{-2}}\ , \tag{26b}$$

$$\sigma'_{I,4}=\frac{1}{\sigma_G^{-1}+\sigma_I^{-1}}+\frac{\sigma_I}{[1+(q\Delta t)^{\beta}]^{-1}+[1+(2q\Delta t)^{\beta}]^{-1}}\ , \tag{27a}$$

$$\sigma'_{I,4}=\frac{1}{\sigma_G^{-1}+\sigma_I^{-1}}+\frac{\sigma_I}{[1+(q\Delta t)^{\beta/2}]^{-2}+[1+(2q\Delta t)^{\beta/2}]^{-2}}\ , \tag{27b}$$

$$\sigma'_{I,5}=\frac{\sigma_I}{1+[1+(2q\Delta t)^{\beta}]^{-1}}+\frac{\sigma_I}{[1+(q\Delta t)^{\beta}]^{-1}+[1+(3q\Delta t)^{\beta}]^{-1}}\ , \tag{28a}$$

$$\sigma'_{I,5}=\frac{\sigma_I}{1+[1+(2q\Delta t)^{\beta/2}]^{-2}}+\frac{\sigma_I}{[1+(q\Delta t)^{\beta/2}]^{-2}+[1+(3q\Delta t)^{\beta/2}]^{-2}}\ , \tag{28b}$$

$$\sigma'_{I,6}=\frac{\sigma_I}{1+[1+(3q\Delta t)^{\beta}]^{-1}}+\frac{\sigma_I}{[1+(q\Delta t)^{\beta}]^{-1}+[1+(q2\Delta t)^{\beta}]^{-1}}\ , \tag{29a}$$

$$\sigma'_{I,6}=\frac{\sigma_I}{1+[1+(3q\Delta t)^{\beta/2}]^{-2}}+\frac{\sigma_I}{[1+(q\Delta t)^{\beta/2}]^{-2}+[1+(2q\Delta t)^{\beta/2}]^{-2}}\ , \tag{29b}$$

$$\sigma'_{I,7}=\frac{\sigma_I}{1+[1+(q\Delta t)^{\beta}]^{-1}}+\frac{\sigma_I}{[1+(q2\Delta t)^{\beta}]^{-1}+[1+(3q\Delta t)^{\beta}]^{-1}}\ , \tag{30a}$$

$$\sigma'_{I,7}=\frac{\sigma_I}{1+[1+(q\Delta t)^{\beta/2}]^{-2}}+\frac{\sigma_I}{[1+(2q\Delta t)^{\beta/2}]^{-2}+[1+(3q\Delta t)^{\beta/2}]^{-2}}\ . \tag{30b}$$

We assume the renormalized conductance $\sigma'_I$ of the cluster bond to be given by the algebraic average

$$\sigma'_I=\sum_{i=1}^{7} C_i\sigma'_{I,i}\ . \tag{31}$$

Relationships (24)–(31) present the renormalization function $\sigma'_I=R_I(\sigma_G,\sigma_I,\Delta t,q)$ for the conductance of the cluster bond.

The time increment $\Delta t$ is renormalized to be the time period $\Delta t'$ in which the growth proceeds from the bottom to the top within the cell. Here the time increment is defined to be the time period between the growth of one bond and the growth of the next bond. The renormalized time increments for the configurations (1)–(7) in Fig. 1 are given by

$$\begin{aligned}
2\Delta t'_1&=2\Delta t\ ,\\
2\Delta t'_2&=3\Delta t\ ,\\
2\Delta t'_3&=3\Delta t\ ,\\
2\Delta t'_4&=3\Delta t\ ,\\
2\Delta t'_5&=4\Delta t\ ,\\
2\Delta t'_6&=4\Delta t\ ,\\
2\Delta t'_7&=4\Delta t\ .
\end{aligned} \tag{32}$$

It is assumed that the renormalized time increment $\Delta t'$ is given by the mean value

$$\Delta t'=\sum_{i=1}^{7} C_i\Delta t'_i\ . \tag{33}$$

Relationships (32) and (33) give the renormalization function $\Delta t'=\mathcal{R}_t(\sigma_G,\sigma_I,\Delta t,q)$ for the time increment. Equations (6)–(8) are solved simultaneously. We find three fixed points $(1/\sigma_G^*,0,0)$, $(1,1,0)$, and $(1/\sigma_G^*,0,1)$ in the parameter space $[1/\sigma_G,1/\sigma_I,v/(1+v)]$. In the limit of $v\rightarrow 0$ (the early stage of development), viscous fingering at a finite viscosity ratio is reproduced. The crossover occurs from the DLA fractal to the dense pattern [4]. At the fixed point (1,1,0), the growth probability becomes uniform over all the surface bonds. The fixed point (1,1,0) corresponds to the Eden model, and is designated the Eden point. Fixed point $(1/\sigma_G^*,0,0)$—the first DLA point—gives the viscous finger at an infinite viscosity ratio with no chemical dissolution. Fixed point $(1/\sigma_G^*,0,1)$—the second DLA point—gives the viscous finger at an infinite viscosity ratio with chemical dissolution. This second DLA point can be obtained after a sufficiently long period of time. As time is increased, the chemical dissolution causes the pore size to become larger. After an infinite period of time, the mobility ratio between the two fluids becomes infinity. Therefore, the second DLA point is due to the chemical dissolution, and is different from the first DLA point. The first DLA point is the usual fixed point in viscous fingering at a finite viscosity ratio. The pore size of branches in a porous medium remains a constant value with increasing time. However, at the second DLA point, the pore size of branches in a porous medium is large when compared to that of the initial stage.

We study the stability of the fixed points in a three-parameter space $[1/\sigma_G,1/\sigma_I,v/(1+v)]$. To find the global flow diagram in the three-parameter space, we choose a point in the parameter space and, using (6)–(8), calculate the renormalized surface conductance, the renormalized conductance of the cluster bond, and the renormalized time increment. This produces a new point

$[1/\sigma_G', 1/\sigma_I', v'/(1+v')]$. We repeat this process to find the next point, and continue until we approach a stable fixed point. Figs. 2 and 3 show, respectively, the renormalization flows for models A and B. The fixed points coincide in models A and B. The renormalization flows show a similar behavior in models A and B qualitatively. Quantitatively, the renormalization flows in models A and B differ somewhat. We can determine the stabilities of the three fixed points: the first DLA point, the Eden point, and the second DLA point. The first DLA point and the Eden point are unstable fixed points. The second DLA point is stable in every direction. All the renormalization flows eventually merge into the second DLA point. Figure 4 shows the global flow diagram of the case with the same viscosity in the two-parameter space $[1/\sigma_I, v/(1+v)]$. There are two fixed points: the Eden point (1,0) and the second DLA point (0,1). Due to chemical dissolution, a crossover occurs from the dense cluster to the DLA pattern. By introducing chemical dissolution into viscous fingering, the Eden point becomes unstable—allowing a crossover from the Eden point to the second DLA point.

We propose the following scaling ansatz along the crossover lines:

$$M(r,\mu,v)=r^{d_f}F_1(\mu r^{\phi_1})F_2(v^{1/\beta}r^{\phi_2}) , \tag{34a}$$

with

$$F_1(x)\approx \begin{cases} 1 & \text{if } x \ll 1 \\ x^{(d-d_f)/\phi_1} & \text{if } x \gg 1 , \end{cases} \tag{34b}$$

and

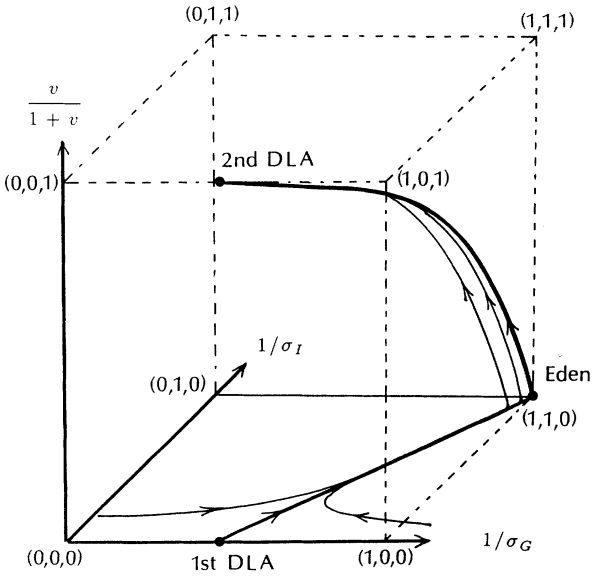


FIG. 2. Global flow diagram of model A in three-parameter space $[1/\sigma_G, 1/\sigma_I, v/(1+v)]$. There are three fixed points: the first DLA point, the Eden point, and the second DLA point. All the renormalization flows are eventually sucked into the second DLA point. In the limit of $v \to 0$, viscous fingering at a finite viscosity ratio is reproduced.

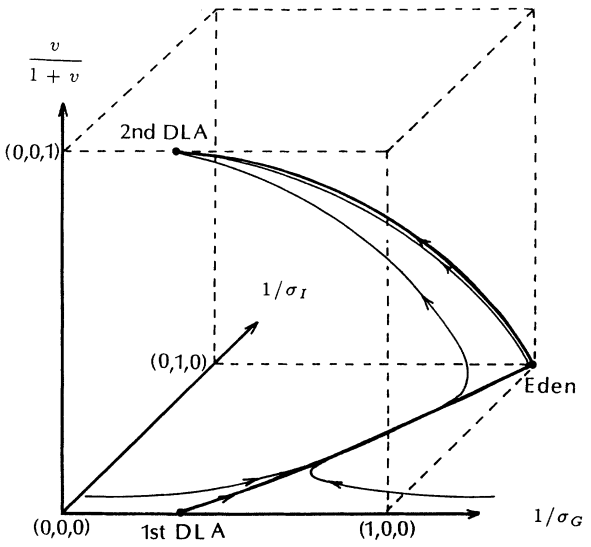


FIG. 3. Global flow diagram of model B in the three-parameter space $[1/\sigma_G, 1/\sigma_I, v/(1+v)]$.

$$F_2(x)\approx \begin{cases} 1 & \text{if } x \ll 1 \\ x^{(d_f-d)/\phi_2} & \text{if } x \gg 1 , \end{cases} \tag{34c}$$

where $F_1$ is the scaling function for the first stage of the crossover (from the first DLA point to the Eden point), $F_2$ the scaling function for the second stage of the crossover (from the Eden point to the second DLA point), $M$ the mass of the cluster, $r$ the radius of gyration, $\mu$ the initial viscosity of the injected fluid, $d$ the embedding dimensions, and $d_f$ the fractal dimension of the DLA pattern. The scaling function for the first stage of the crossover corresponds to that of viscous fingering at a finite viscosity ratio.

In an experiment with the same viscosity ($\mu=1$), only

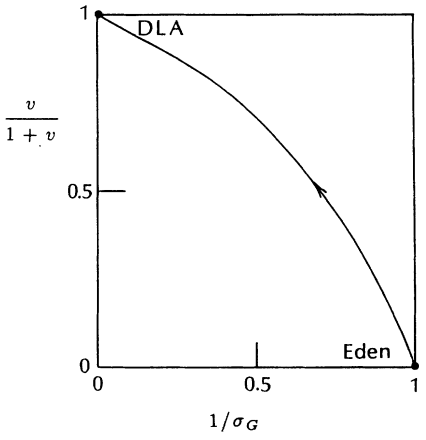


FIG. 4. Global flow diagram of model A in the two-parameter space $[1/\sigma_I, v/(1+v)]$ when the viscosity of the injected fluid is the same as that of the displaced fluid. The crossover occurs from the Eden fixed point from the second DLA fixed point.

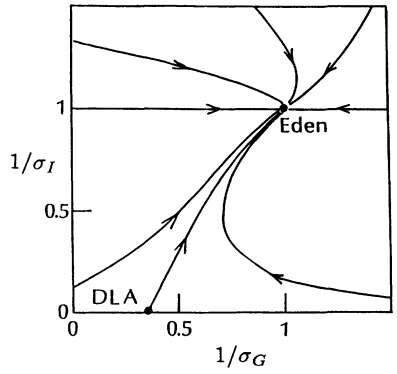


FIG. 5. Global flow diagram in the two-parameter space $(1/\sigma_G, 1/\sigma_I)$ in the no-reaction regime. The global flow diagram corresponds to viscous fingering at a finite viscosity ratio.

the second stage of the crossover occurs. In order to quantify this crossover behavior, we define a crossover $\phi$ and a crossover radius $r_c$. We propose the scaling ansatz along the crossover line from the Eden point to the second DLA point,

$$M(r,v)=r^d F(v^{1/\beta} r^{\phi}) , \tag{35a}$$

with

$$F(x)\approx \begin{cases} 1 & \text{if } x \ll 1 \\ x^{(d-d_f)/\phi} & \text{if } x \gg 1 , \end{cases} \tag{35b}$$

where the subscript 2 drops out for both the scaling function and the crossover exponent. The crossover radius $r_c$ scales as

$$r_c \sim (v^{1/\beta})^{-1/\phi} . \tag{36}$$

The crossover exponent $\phi$ is found by linearizing the renormalization equations and calculating the eigenvalues. We obtain $\phi \cong 1.63$, and find that the crossover radius depends on the total volume $v$ of the injected fluid. Because the crossover radius decreases with $v$, the evolution from fingering pattern to DLA fractal accelerates as the flow rate increases. The crossover from dense pattern to DLA pattern will begin earlier if the flow rate is increased. It has been proven that the pattern formed by chemical dissolution evolves to a DLA fractal as the flow rate increases [1,2]. The chemical dissolution reverses the direction of the crossover in the viscous fingering at a finite viscosity ratio. Figure 5 shows the renormalization flows without the reaction. The crossover occurs from DLA fractal to dense structure. The scaling form of the crossover is that for viscous fingering at a finite viscosity ratio (see Ref. [4]).

## IV. EFFECT OF FINITE CONCENTRATION

We examine how the finite concentration of the reactant affects the pattern. At a late stage of the dissolution process, the dissolving power becomes limited by the finite concentration of the reactant. Because of consumption of the reactant, the pore size of the branches cannot continue to increase. One would expect that a finite concentration would stabilize the pattern, i.e., would favor the Eden limit. Let us examine how finite concentration of reactant affects the workings of model B. The concentration $c$ of the reactant decreases as the reactant is spent. We assume the following relationship between reactant concentration and time:

$$c = c_0 \exp[-b(t-t_0)] , \tag{37}$$

where $c_0$ is the initial concentration of the reactant and $1/b$ the time constant that characterizes the spending of the reactant. By substituting back into Eq. (4), replacing $C_0$ with $C$ of (37), we obtain an expression of mobility that takes into account the finite concentration effect.

We study how finite concentration affects pattern formation by using the above renormalization-group method. For simplicity's sake, we consider a case with the same viscosity $\mu=1$, i.e., the viscosity of the reactive injection fluid equals that of the displaced fluid. Figure 6 shows the fixed points and the renormalization flows in the two-parameter space $[1/\sigma_I, v/(1+v)]$. We find the three nontrivial fixed points (1,0), (0,1), and (1,1). The fixed point (1,0) corresponds to the first Eden point and represents a dense structure. The fixed point (0,1) corresponds to the second DLA point and represents a DLA fractal caused by chemical dissolution. The fixed point (1,1) is the new point that is generated by the finite concentration effect of the reactant. The fixed point (1,1) represents a dense structure because the mobility $\sigma_I$ of the reactive injection fluid has become one. We call this fixed point the second Eden point.

The three renormalization flows 1, 2, and 3 are the initial conditions ($b=0$, $\Delta t=10^{-4}$, $c_0=1$), ($b=0.2$, $\Delta t=10^{-4}$, $c_0=1$), and ($b=0.5$, $\Delta t=10^{-4}$, $c_0=1$), respectively. The renormalization flow 1 corresponds to

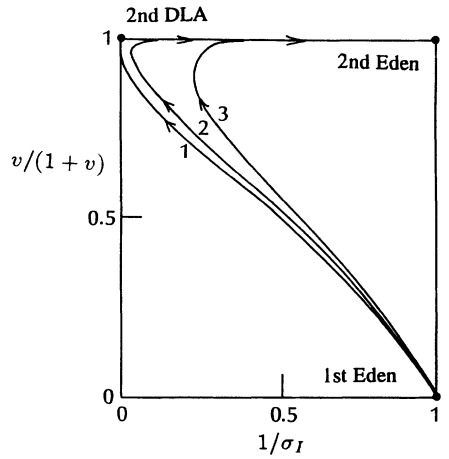


FIG. 6. Global flow diagram in the two-parameter space $[1/\sigma_I, v/(1+v)]$ for the finite concentration effect of the reactant when the viscosity of the injected fluid is consistent with that of the displaced fluid. The two-stage crossover phenomena occur from the Eden fixed point, through the DLA fractal fixed point, to the Eden fixed point.

the case in which the finite concentration effect is not taken into account. The renormalization flows 2 and 3 are eventually collapsed into the second Eden point. As the time constant $1/b$ is decreased, i.e., as the reactant is consumed more rapidly, the renormalization flow deviates from the second DLA point, and it becomes increasingly unlikely that a DLA fractal caused by chemical dissolution will appear. If there is an appropriate time constant $1/b$ ($b \approx 0.2$), the two-stage crossover (from Eden, through DLA fractal, to Eden) will occur. We find that a finite concentration of the reactant stabilizes the pattern, i.e., favors the Eden limit.

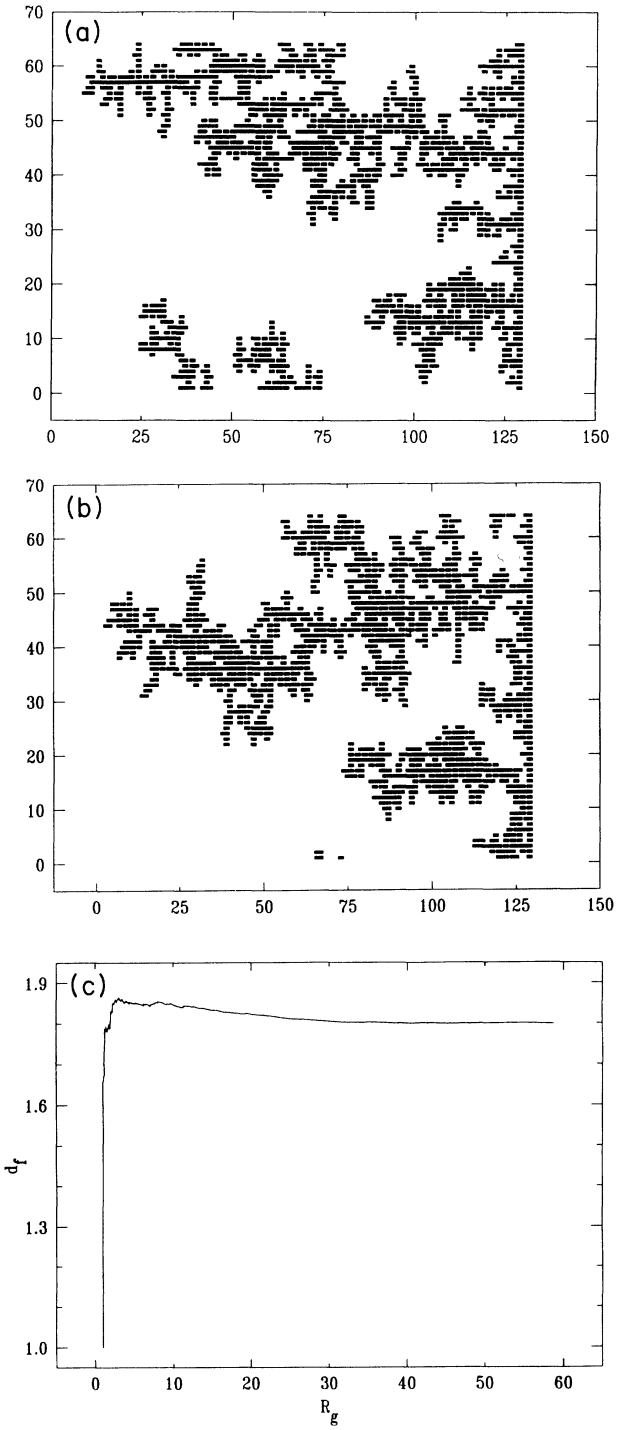


FIG. 7. Simulations for (a) $P_0=10^{-3}$ and (b) $P_0=1$ for a $128\times64$ square lattice, and 1000 Monte Carlo steps. (c) The dependence on cluster size of the fractal dimension $d_f$ with $P_0=10^{-3}$.

## V. SIMULATION

We have checked the results of the present PSRG approach for the case $\mu=1$ by direct numerical simulation. We find (i) that the asymptotic pattern is DLA, and (ii) that the pattern obtained is independent of injection pressure. Our simulations were performed for a $128\times64$ square lattice with periodic boundary conditions in the vertical direction (Fig. 7). The pressure on the left edge is fixed at zero, and on the right edge at $P_0$. At each time step, we solve Eqs. (1) by the over-relaxation method. For each interface bond $i$, we calculate the current $q_i$; we then occupy bond $i$ with probability $q_i / \sum_j q_j$, where the index $j$ runs over all the interface bonds. The first Monte Carlo step is completed by updating the mobility using Eq. (2). Figures 7(a) and 7(b) show the pattern after 1000 Monte Carlo steps for the cases $P_0=10^{-3}$ and 1, respectively. We see no essential difference between these two patterns. As predicted by the PSRG, the injection pressure changes only the time scale of the pattern development. We also notice that the pattern resembles DLA. To check this possibility, we calculated the fractal dimension $d_f$ of the pattern using the box-counting method. We find (Fig. 7(c)] that $d_f$ approaches 1.7, which is consistent with known results for DLA.

## VI. SUMMARY

Using three-parameter PSRG equations, we have analyzed the morphological changes that take place in viscous fingers when a reactive injection fluid brings on chemical dissolution. In the mass-transfer-limit regime, we find that two-stage crossover phenomena occur at an increasing rate when the viscosity of the injection fluid is low, i.e., (i) from DLA pattern to dense pattern due to finite viscosity effect, and (ii) from dense pattern to DLA pattern due to chemical dissolution. We have presented the scaling forms for two-stage crossovers and have calculated crossover exponent $\phi$ and crossover radius $r_c$. We have also studied how a finite concentration of the reactant affects the pattern. We find that a finite concentration stabilizes the pattern, i.e., favors the Eden limit, and, because of chemical dissolution, crossover from DLA fractal to dense structure occurs.

## ACKNOWLEDGMENTS

We are grateful to A. Coniglio, G. Daccord, and N. Quirke for useful discussions. This work was supported by the NSF and BP.

*Present address: HLRZ, Forschungszentrum Jülich, Postfach 1913, D-5170 Jülich, Germany.

[1] G. Daccord, Phys. Rev. Lett. **58**, 479 (1987).

[2] G. Daccord and R. Lenormand, Nature **325**, 41 (1987); see also M. L. Hoefner and H. S. Fogler, AIChE J. **34**, 45 (1988); G. Daccord, E. Touboul, and R. Lenormand, SPE Prod. Eng. **4**, 63 (1989). Color photographs displaying the phenomenon of chemical dissolution appear in Plate 11 of D. Stauffer and H. E. Stanley, *From Newton to Mandelbrot: A Primer in Theoretical Physics* (Springer-Verlag, Heidelberg, 1990), and in Plate 41 of E. Guyon and H. E. Stanley, *Les Formes Fractales* (Palais de la Decouverte, Paris, 1991) [English translation: *Fractal Forms* (Elsevier, Amsterdam, 1991)]. See also the review G. Daccord, in *The Fractal Approach to Heterogeneous Chemistry,* edited by D. Avnir (Wiley, New York, 1989).

[3] See, e.g., P. Meakin, in *Phase Transitions and Critical Phenomena,* edited by C. Domb and J. L. Lebowitz (Academic, New York, 1988), Vol. 12; J. Feder, *Fractals* (Pergamon, New York, 1988); *Random Fluctuations and Pattern Growth,* edited by H. E. Stanley and N. Ostrowsky (Kluwer Academic, Dordrecht, 1988); T. Vicsek, *Fractal Growth Phenomena* (World Scientific, Singapore, 1989); *Correlations and Connectivity: Geometric Aspects of Physics, Chemistry and Biology,* edited by H. E. Stanley and N. Ostrowsky, Proceedings of the 1990 Cargèse NATO Advanced Study Institute, Ser. E: Applied Sciences Vol. 188 (Kluwer, Dordrecht, 1990); *Fractals and Disordered Systems,* edited by A. Bunde and S. Havlin (Springer-Verlag, Berlin, 1991).

[4] J. Lee, A. Coniglio, and H. E. Stanley, Phys. Rev. A **41**, 4589 (1990).

[5] T. Nagatani, Phys. Rev. A **40**, 7286 (1989).

[6] T. Nagatani and H. E. Stanley, Phys. Rev. A **41**, 3263 (1990).

[7] T. Nagatani and H. E. Stanley, Phys. Rev. A **43**, 2963 (1991).

[8] T. Nagatani, J. Lee, and H. E. Stanley, Phys. Rev. Lett. **66**, 616 (1991).

[9] G. Daccord, O. Liétard, and R. Lenormand (unpublished).

[10] V. G. Levich, *Physiochemical Hydrodynamics* (Prentice-Hall, Englewood Cliffs, NJ, 1962).

[11] We also used the geometric average, and found no qualitative difference.